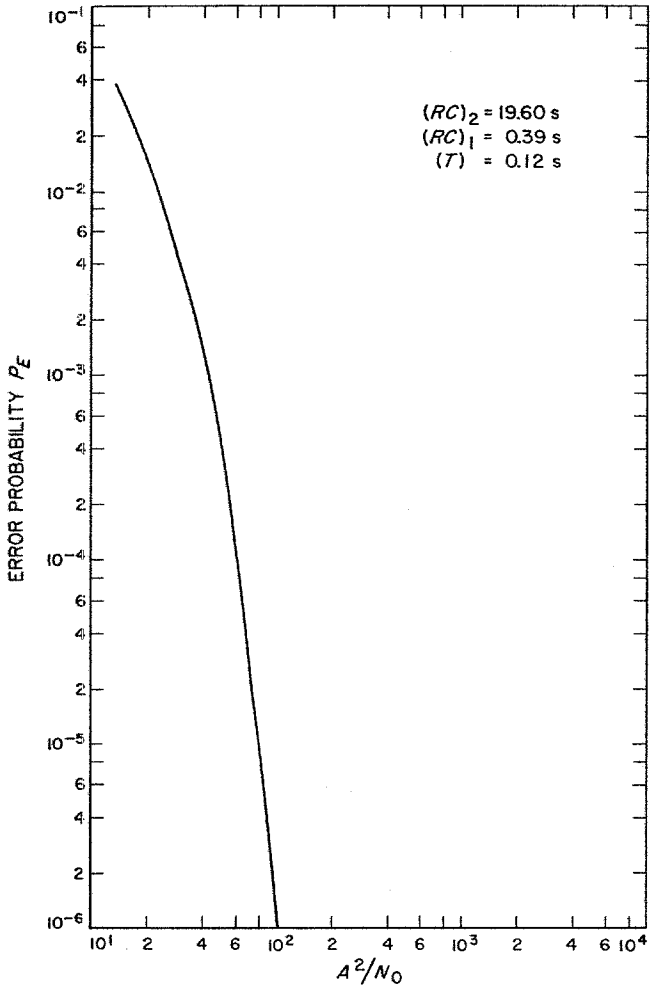

Fig. 3. Probability of error versus the ratio A^2/N_0

3. Effect of the High-Pass Filter

In order to visually ascertain the effect of the high-pass filter on the digital dump detector, the probability of error was computed for three values of R_1C_1 and two values of A^2/N_0 as a function of the ratio R_2C_2/R_1C_1. The results are plotted in Fig. 2. Figure 3 illustrates the probability of error as a function of A^2/N_0 for the parameters $R_1C_1 = 0.39$ s and $R_2C_2 = 19.6$ s.

B. Digital Data-Transition Tracking Loops,

W. C. *Lindsey and R. C. Tausworthe*

1. Introduction

Recently, considerable interest has developed in the problem of tracking data transitions in digital communication systems. The application of this technique is to provide the receiver with an accurate estimate of symbol synchronization, i.e., the instants in time when the modulation may change states. In so-called single-channel (Ref. 1) digital communication systems where symbol and subcarrier synchronization are derived from the recovered modulation, such a method offers a saving in transmitter power over the so-called two-channel (Ref. 2) system where a separate timing signal is transmitted for synchronization purposes. An example of the two-channel system is *Mariner IV* telecommunication system, while an example of a single-channel system is the *Mariner* Mars 1969 telecommunication system in both the high and low data-rate modes. This article presents an analysis of a particular type of symbol-tracking device. In subsequent analyses, we intend to investigate other types of devices for comparison. The results are useful in designing synchronizing circuitry for a wide variety of digital systems, e.g., block decoders and sequential decoders.

2. System Model

A block diagram of a digital data-transition tracking loop is depicted in Fig. 4. The tracking loop consists of two branches: an "in-phase" branch, the upper half, and a "mid-phase" branch, the lower half. These two branch outputs, viz., $I(t_n)$ and $M(t_n)$, are fed into a phase detector, the loop multiplier, producing the signal $e(t_n)$ which is filtered by the loop filter $F(s)$. The output, say $v(t)$, of $F(s)$ is used to control the instantaneous frequency and phase of the voltage-controlled oscillator (VCO). The VCO output is used to control a time generator which produces the time ticks t_n for sampling the output of the in-phase and mid-phase filters. The decision device accepts the output from the in-phase filter and announces "+1" if the input is greater than zero and "−1" if the input is less than zero. This information is fed into the transition detector whose outputs are either "+1," "−1," or "0." Since the transition "value" depends on the input up until time t_n, whereas the mid-symbol integral depends only on times up to $t_n - T/2$, it is necessary to delay the mid-symbol integral by $T/2$ seconds to give a number $M(t_n)$ to the loop. This effectively inserts the function $\exp(-T_s/2)$ into the open-loop transfer function; but, as we shall assume $w_LT << 1$, its effect on loop operation is negligible and is hence omitted in the analysis to follow. The transition value "+1" is assumed if the data sequence goes from plus to minus, i.e., a negative-going transition occurs. If no transition in the data takes place, the output $I(t_n)$ is set to zero. The mid-phase (MP) filter is, in effect, the error channel of the loop, and the algebraic sign of its output is switched in accordance with signal $I(t_n)$ to produce the so-called tracking loop S-curve. The input signal $x(t)$, which in practice is the output of a subcarrier tracking loop, is assumed to be the sum of a signal $s(t)$ plus

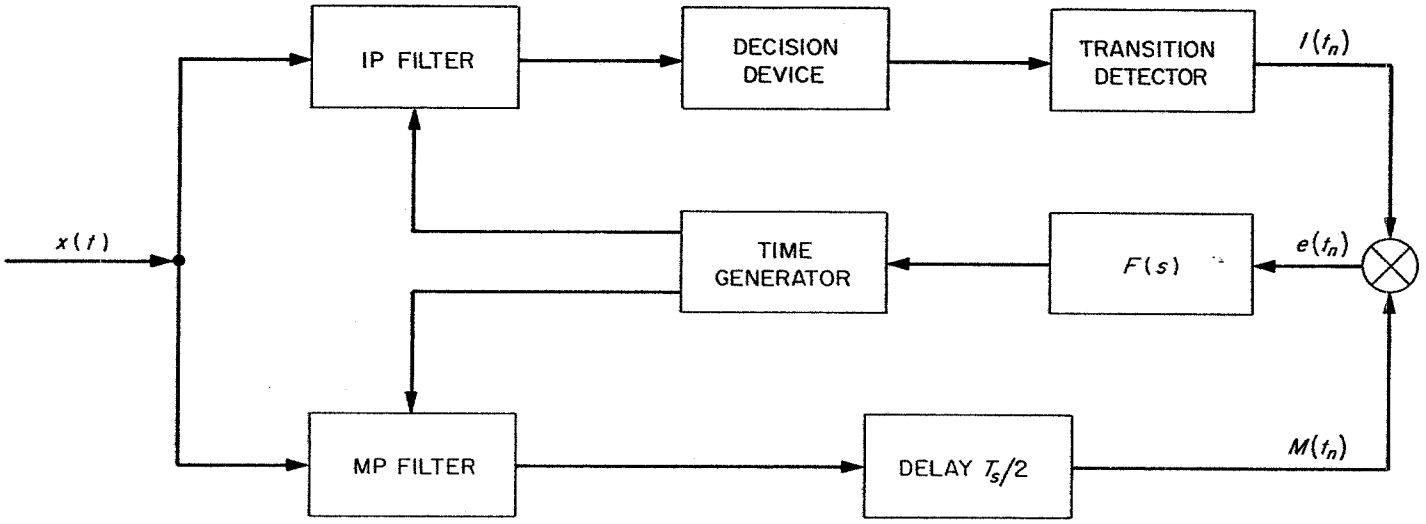

Fig. 4. Data-transition tracking loop

additive white Gaussian noise $n(t)$. In what follows we shall develop an analysis which enables one to design such a loop, determine the range in data rate and signal-to-noise ratio in the loop bandwidth, etc., for which the loop will provide the necessary timing accuracy required for symbol synchronization.

In practice, a wide range of operating signal and noise levels can be tolerated since the tracking loop can be implemented in the hybrid digital/analog domain using high-speed analog/digital and digital/analog interfaces. This conceivably can allow for implementation of loop bandwidths on the order of a few tenths to a few thousandths of a cycle. Moreover, the loop filter, being digital, may be implemented as a perfect integrator (i.e., a loop which includes one first- and one second-order component, Ref. 3) so that operational problems due to false lock, static phase-error, etc., are minimized. In what follows, we quantitatively describe the loop and determine its behavior as a function of three parameters, viz., the energy per symbol E_s, noise spectral density N_0, and the ratio δ_s of the symbol rate $R_s = 1/T_s$ to the loop bandwidth w_L as a measure of performance. The mean-square jitter about the loop's lock point is evaluated.

3. System Analysis and Design Trends

It is assumed that the input signal $x(t)$ consists of a sequence of pulses of time duration T and random amplitude $\pm A$, where the probability of $+A$ equals the probability of $-A$, and that the additive noise $n(t)$ is white and Gaussian with a single-sided spectral density of N_0 watts/cycle. Thus

$$x(t) = \sum_n b_n u(t - nT - \epsilon) + n(t) \qquad (1)$$

where

$$u(t) = 1, \text{if } 0 \leq t \leq T$$

$$= 0, \text{elsewhere}$$

and ϵ is the random epoch to be estimated. In Eq. (1), $b_n = \pm A$ and $p(+A) = p(-A) = \frac{1}{2}$.

The procedure which we use to analyze loop behavior is to develop an equivalent model of the loop from which the nonlinear theory of tracking loops, viz., the Fokker–Planck apparatus, may be used to specify loop performance. This involves two computations: (1) determination of loop S-curve on the average as a function of the normalized offset $\lambda = \tau/T$ from the lock point $\tau = \epsilon - \hat{\epsilon}$, and (2) determination of the spectral density about the origin of the equivalent noise as a function of the normalized offset λ. We shall refer to this spectral density as $S(\omega, \lambda)$ and the S-curve as $g(\lambda)$. We assume that the noise which disturbs the loop is white and Gaussian with a double-sided spectral density of $S(0, \lambda)$ watts/cycle. For all practical purposes, then, the equivalent transition tracking loop of Fig. 4 may be replaced by the mathematically equivalent loop illustrated in Fig. 5. In Fig. 5, the spectral density of $n_\lambda(t_n)$ is denoted by $S(0, \lambda)$, and K is the product of the VCO gain constant and the gain of the loop's phase detector. Obviously, $S(0, \lambda)$ is monotonically increasing in λ, since the further away from the lock point ($\lambda = 0$) the more noise one has to contend with in $I(t_n)$.

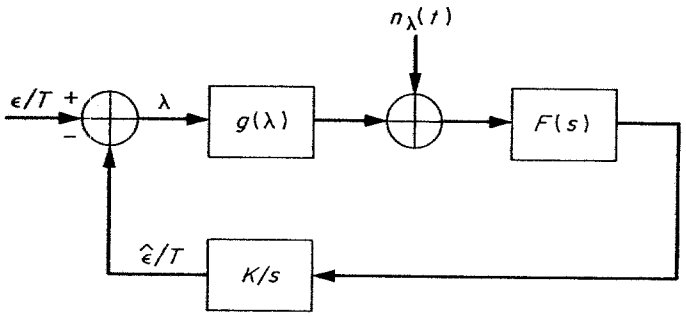

Fig. 5. Equivalent data-transition tracking loop model

This is due to the fact that more errors are made in the "in-phase" branch which, in effect, injects more noise into the multiplier of Fig. 4.

If little data degradation can be tolerated, then extreme accuracy is required in establishing symbol synchronization. Thus, the value of $S(0,\lambda)$ is essentially the noise spectral density seen by the loop at $\lambda = 0$, viz., $S(0,0)$. If one assumes that the in-phase filter and the mid-phase filter are perfect integrators with integration time T seconds, then it may be shown that the S-curve is expressed by

$$g(\lambda) = AT\lambda\,[1 - 2P_{E_t}(\lambda)], \qquad |\lambda| \leq \frac{1}{2} \tag{2}$$

where $P_{E_t}(\lambda)$ is the probability of detecting a transition incorrectly, viz.,

$$P_{E_t}(\lambda) = \text{Erfc}\,\{[2R_s(1 - 2|\lambda|)]^{1/2}\} \tag{3}$$

and $R_s = A^2T/N_0$. By Erfc (x) is meant the function

$$\text{Erfc}\,(x) = \frac{1}{(2\pi)^{1/2}}\int_x^\infty \exp(-z^2/2)\,dz \tag{4}$$

Figure 6 illustrates the S-curve $g(\lambda)$ for various values of R_s. It is seen that, for large R_s, the curves are linear while for smaller R_s the curves are highly dependent upon R_s. Also, it may be shown that

$$S(0,0) = \frac{N_0T}{4}\left(1 + \frac{R_s}{2}\frac{1}{2}\left\{\frac{1}{\pi^{1/2}}\exp(-R_s) + R_s\,[1 - P_{E_t}(0)]\right\}^2\right) = N_0Th/4 \tag{5}$$

in which h represents the bracketed quantity. Obviously, as R_s approaches infinity

$$S(0,0) = N_0T/4 \tag{6}$$

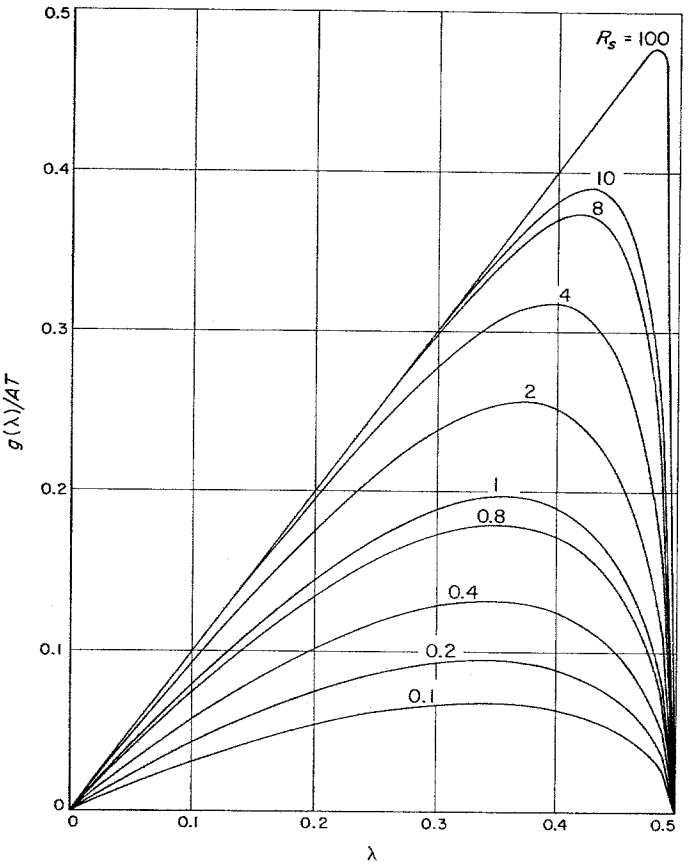

Fig. 6. The function $g(\lambda)/AT$ versus λ for various R_s

as it should, i.e., h approaches unity.

The stochastic differential equation which relates the pertinent parameters to the loop model in Fig. 5 may be written as (assuming zero static timing error)

$$\dot{\lambda} = KF(p)\,[ATg(\lambda) + n(t)] \tag{7}$$

where $\lambda = \tau/T = (\epsilon - \hat{\epsilon})/T$. Since solving stochastic differential equations is meaningful only in the probabilistic sense, we seek to determine the probability distribution $p(\lambda)$ by the Fokker–Planck method (Ref. 3). Without belaboring the details of the derivation, we have that

$$p(\lambda) = N\exp\left\{-\frac{2R_s\delta_s}{h}\int_{-1/2}^{\lambda} x\,[1 - 2P_{E_t}(x)]\,dx\right\}, \qquad |\lambda| \leq \frac{1}{2} \tag{8}$$

where N is chosen such that

$$\int_{-1/2}^{1/2} p(\lambda) = 1 \tag{9}$$

Table 1. Values of $p(\lambda)$ for various values of λ and δ_s with $R_s = 0.8$

δ_s	$\lambda = 0$	$\lambda = 0.125$	$\lambda = 0.250$	$\lambda = 0.375$	$\lambda = 0.50$
10^1	6.1×10^{-1}	6.1×10^{-1}	6.1×10^{-1}	6.1×10^{-1}	6.1×10^{-1}
10^2	5.2×10^{1}	1.3×10^{1}	2.5×10^{-1}	3.1×10^{-4}	2.7×10^{-8}
10^3	1.6×10^{2}	2.5×10^{-4}	1.0×10^{-21}	0	0
10^4	5.2×10^{2}	0	0	0	0
10^5	1.6×10^{3}	0	0	0	0

and $\delta_s = 1/Tw_L = R_s/w_L$. The parameter w_L is the loop bandwidth. It is clear from Eq. (8) that, for small $P_{E_t}(x)$, i.e., large R_s, $p(\lambda)$ becomes Gaussian with variance, as determined from Eq. (8), of

$$\sigma_\lambda^2 = \frac{h}{2R_s\delta_s} = \frac{hN_0w_L}{2A^2} \tag{10}$$

In the linear region of operation, the variance of the normalized timing error is proportional to the signal-to-noise ratio in the loop bandwidth w_L.

A table of values for the distribution $p(\lambda)$ is illustrated in Table 1 for $R_s = 0.8$, typical of *Mariner* Mars 1969, for various values of δ_s. It can be seen that $p(\lambda)$ becomes uniformly distributed as $\delta_s R_s = A^2/N_0w_L$ approaches zero. The variance of the normalized timing error, given by

$$\sigma_\lambda^2 = 2\int_0^{1/2} \lambda^2 p(\lambda)\, d\lambda \tag{11}$$

has been obtained using numerical integration; the results are illustrated in Fig. 7 for a wide range of design parameters.

As an alternate mechanization of the tracking loop, it is possible to improve loop performance by reducing the noise variance $S(0,\tau)$ at the expense of changing the S-curve. This may be accomplished by integrating in the mid-phase channel only over a portion of the symbol time, say w seconds. In this case it may be shown that the S-curve is given by

$$g(\lambda) = \begin{cases} AT\lambda\,[1 - 2P_{E_t}(\lambda)], & 0 \leq \lambda \leq w/2T \\ Aw\,[1 - 2P_{E_t}(\lambda)], & w/2T \leq \lambda \leq w/T \end{cases} \tag{12}$$

and the corresponding values of the noise spectral density about $w = 0$ is given by

$$S(0,0) = \frac{N_0wh'}{4} \tag{13}$$

Thus, it would appear that the noise $S(0,0)$ may be made arbitrarily small by allowing w to approach zero; however, the problem of symbol slipping around the lock point begins to degrade the loop's tracking capability. Figure 8 places into evidence the deleterious effects on the S-curve when $w = T/2$ for various values of R_s and λ. Obviously, the smaller the w the larger is the probability

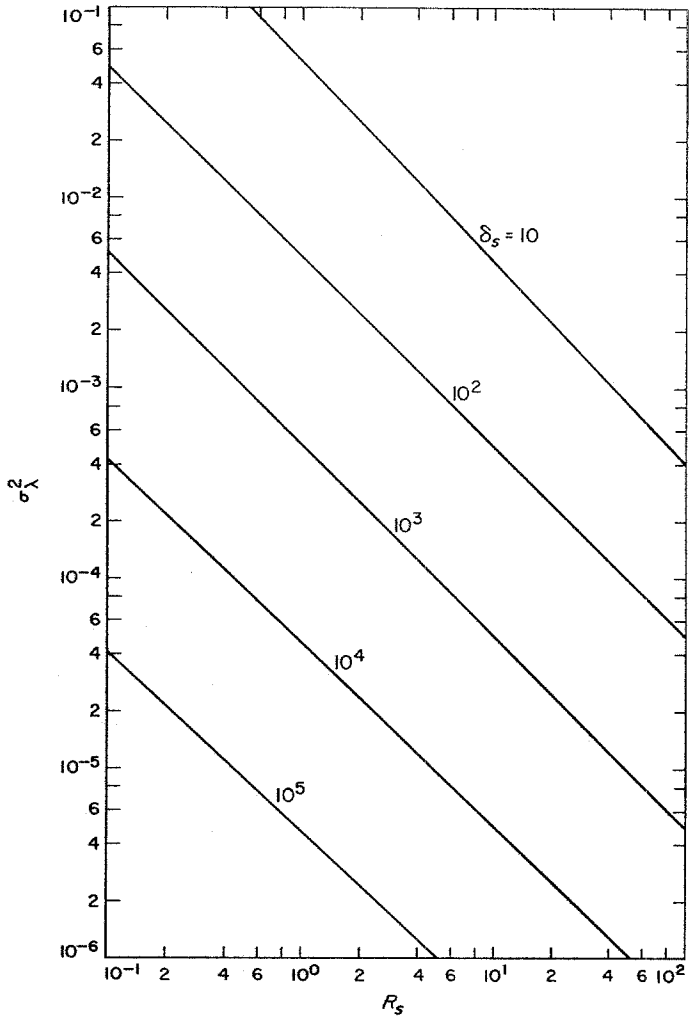

Fig. 7. Variance σ_λ^2 of the normalized jitter versus R_s for various values of δ_s

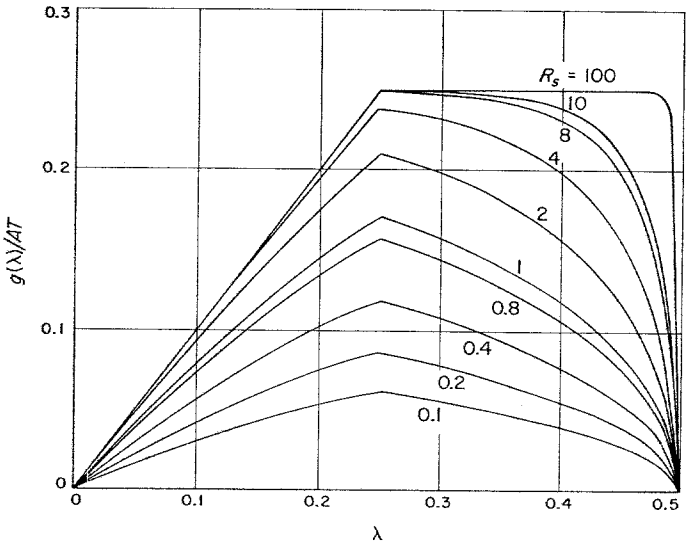

Fig. 8. The function $g(\lambda)/AT$ versus λ for various R_s with $w = T/2$

of slip for a given signal-to-noise ratio. It would appear, then, that there exists a "best" w for a given mean time to first symbol slip. This particular problem is best treated by evaluating the mean time to first slip as a function of w, R_s and δ_s. We shall not elaborate upon this here; however, in a later article we shall address this problem.

In the linear region of loop operation, the variance of the normalized loop jitter is thus given by

$$\sigma_\lambda^2(w) = \frac{wh'}{2R_s} \cdot w_L \tag{14}$$

Comparing this with the situation $w = T$ (i.e., integration over the full symbol time in the error channel) we have

$$\frac{\sigma_\lambda^2(w)}{\sigma_\lambda^2} = \frac{h'}{h} \cdot \frac{w}{T} \tag{15}$$

in the linear region. For the cases of practical interest, $h' \simeq h$, so the improvement in normalized jitter is approximately

$$\frac{\sigma_\lambda^2(w)}{\sigma_\lambda^2} \simeq \frac{w}{T} \tag{16}$$

If $w = T/2$, then there is an approximate 3-dB improvement, i.e.,

$$\frac{\sigma_\lambda^2(T/2)}{\sigma_\lambda^2} \simeq \frac{1}{2} \tag{17}$$

As before, we may write the probability density $p(\lambda)$ using Fokker–Planck methods. For the case where the mid-symbol channel integrates over a portion of the symbol time, we find that

$$p(\lambda) = N \exp\left[-\frac{\delta_s R_s}{h'}\int_{-\frac{1}{2}}^{\lambda} g(x)\,dx\right], \qquad |\lambda| \leq \frac{1}{2} \tag{18}$$

where N is again chosen such that

$$\int_{-\frac{1}{2}}^{\frac{1}{2}} p(\lambda)\,dx = 1 \tag{19}$$

At large values of R_s, $p(\lambda)$ again becomes Gaussian; at small R_s, $p(\lambda)$ approaches the uniform distribution. Future work will be devoted to the problem of finding that value of w, say w_0, for which the variance of the distribution given in Eq. (19) is a minimum.

References

1. Lindsey, W. C., "Optimal Design of One-Way and Two-Way Coherent Communications Links," *IEEE Trans. Commun. Technol.*, Vol. COM-14, No. 4, Aug. 1966.
2. Lindsey, W. C., "Determination of Modulation Indexes and Design of Two-Channel Coherent Communication Systems," *IEEE Trans. Commun. Technol.*, Vol. COM-15, No. 2, pp. 229–237, Apr. 1967.
3. Lindsey, W. C., and Tausworthe, R. C., "A Survey of Phase-Locked Loop Theory," in *Recent Advances in Space Communications*. Edited by A. V. Balakrishnan. McGraw-Hill Book Co., New York (to be published).

C. Nonlinear Analysis of Phase-Locked Loops in Cascade, *W. C. Lindsey and C. L. Weber*

1. Introduction

In a wide variety of applications, the phase-lock principle is applied to loops in cascade. For example, in deep space communication systems, extremely accurate two-way Doppler and phase measurements are needed to provide information concerning the relative position and velocity of the spacecraft; i.e., tracking data is needed for orbit determination. Certainly the linear, quasi-linear, linear spectral and Volterra theory discussed previously[2] applies directly; however, these methods of analysis yield only approximate results and do not attempt to get the joint probability distribution of the phase errors, whereby various moments and significant parameters are determined.

[2]Lindsey, W. C., and Tausworthe, R. C., "A Survey of Phase Locked Loop Theory," *Proc. IEEE* (to be published).